Record High Efficiency Single-Walled Carbon Nanotube/Silicon p-n Junction Solar Cells

ARTICLE *in* NANO LETTERS · DECEMBER 2012

Impact Factor: 13.59 · DOI: 10.1021/nl3035652 · Source: PubMed

5 AUTHORS, INCLUDING:

Yeonwoong Jung
Yale University
40 PUBLICATIONS **1,041** CITATIONS
SEE PROFILE

Xiaokai Li
Yale University
15 PUBLICATIONS **318** CITATIONS
SEE PROFILE

NANO LETTERS

Letter

pubs.acs.org/NanoLett

Record High Efficiency Single-Walled Carbon Nanotube/Silicon p–n Junction Solar Cells

Yeonwoong Jung,*[,†,§] Xiaokai Li,[‡,§] Nitin K. Rajan,[∥] André D. Taylor,*[,‡] and Mark A. Reed[†,∥]

[†]Department of Electrical Engineering, Yale University, New Haven, Connecticut, 06520, United States

[∥]Department of Applied Physics, Yale University, New Haven, Connecticut, 06520, United States

[‡]Department of Chemical and Environmental Engineering, Yale University, New Haven, Connecticut, 06520, United States

Supporting Information

ABSTRACT: Carrier transport characteristics in high-efficiency single-walled carbon nanotubes (SWNTs)/silicon (Si) hybrid solar cells are presented. The solar cells were fabricated by depositing intrinsic p-type SWNT thin-films on n-type Si wafers without involving any high-temperature process for p–n junction formation. The optimized cells showed a device ideality factor close to unity and a record-high power-conversion-efficiency of >11%. By investigating the dark forward current density characteristics with varying temperature, we have identified that the temperature-dependent current rectification originates from the thermally activated band-to-band transition of carriers in Si, and the role of the SWNT thin films is to establish a built-in potential for carrier separation/collection. We have also established that the dominant carrier transport mechanism is diffusion, with minimal interface recombination. This is further supported by the observation of a long minority carrier lifetime of ~34 μs, determined by the transient recovery method. This study suggests that these hybrid solar cells operate in the same manner as single crystalline p–n homojunction Si solar cells.

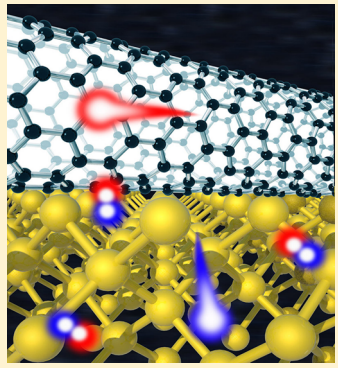

KEYWORDS: *CNT/Si solar cell, hybrid solar cell, photovoltaics, high efficiency, ideality factor, temperature dependency*

Carbon nanotube (CNT)/silicon (Si) hybrid solar cells are a new class of photovoltaic devices which benefits from the superior opto-electronic properties of CNTs[1] coupled with well-established Si photovoltaic technologies. These advantages, further driven by a simple, cost-effective fabrication process have recently stimulated intense research interest.[2−9] A transparent CNT film deposited on a Si wafer functions as a charge carrier collecting conductive electrode and establishes a built-in voltage for separating photocarriers. In this regard, single-walled carbon nanotubes (SWNTs) are more suitable than double- (or multi-) walled carbon nanotubes owing to their tunable/direct band gap energies matching with a wide range of the solar spectrum and better charge carrier transport properties.[1]

Despite the high promise of this approach, many technical/scientific issues remain to be resolved to make this approach more viable for practical applications. The power-conversion efficiency (PCE) of such solar cells needs to be improved, and this should be realized through a cost-effective process. The maximum PCE of SWNT/Si solar cells reported so far[2] remains below 11%, and their device ideality factors are significantly greater than unity, indicating that carrier transport is limited by recombination. Some alternative approaches have been developed to achieve higher efficiency (>12%) by "wetting" SWNT/Si interfaces,[3−6] which rely on the in situ infiltration of acid solutions[3,4] or the control of electronic junctions via an ionic liquid electrolyte.[5,6] These methods, however, suffer from the volatility of the incorporated liquid media; therefore, the "wet-state" efficiency does not represent the intrinsic PCE of solar cells.[10]

Besides the limited PCEs, the underlying transport mechanism of SWNT/Si solar cells is not well-established and remains under debate. This is mainly because SWNTs are mixtures of both semiconducting and metallic nanotubes with inhomogeneous diameters and chiralities,[1] which leads to the complexity in the nature of the electronic junction of SWNT/Si.[2] There are potentially three models of operation: p–n heterojunction,[7−9] metal–semiconductor (MS) Schottky junction,[5] or metal–insulator–semiconductor (MIS) Schottky junction that functions like a p–n homojunction.[4] In the p–n junction model, the SWNT thin film acts as a light-transmitting p-type emitter, and photocarriers are separated under the action of the built-in potential formed by the SWNT (p-type)/Si (n-type) junction. In the MS Schottky junction model, the Schottky barrier formed at the interface of SWNT (M)/Si (S) is responsible for majority carrier-driven rectification. A closely related transport mechanism is the MIS Schottky model, where a thin insulator (I) (typically a few nanometers) is inserted between SWNTs (M) and Si (S). A thin layer of Si near the insulator is inverted, and a photocarriers are separated by the built-in potential formed

Received: September 24, 2012
Revised: November 29, 2012
Published: December 13, 2012

   dx.doi.org/10.1021/nl3035652 | *Nano Lett.* 2013, 13, 95−99

between the insulator (whose Fermi level is pinned to that of the adjacent SWNTs) and the Si.[2] However, due to the significant nonideality of the devices reported so far, clarification of the exact model has been elusive. The purpose of this paper is to elucidate which model is dominant for the devices with near-ideal transport characteristics, which will be very useful to further design/optimize solar cells with improved performance. In this work, we have demonstrated SWNT/Si solar cells with an intrinsic PCE of >11%, greater than any other previously reported CNT/Si solar cells.

SWNT/Si hybrid solar cells were fabricated by depositing p-type SWNT thin films onto n-type Si (doping concentration: $\sim 10^{15}-10^{16}$ cm^{-3}) wafers. High-quality SWNT thin films were fabricated by the "superacid sliding coating method" developed in our laboratories.[11] SWNT ink is prepared by adding chlorosulfonic acid to SWNTs followed by stirring in a nitrogen environment. A drop of the prepared SWNT ink is sandwiched between two slide glasses, which are manually pressed together and are slid across each other in opposite directions. The slides are either slowly dried or gently dipped into deionized water to remove any acid leached out of the film. The resulting film is floated on the top of the deionized water and is ready for transfer to the top of prepatterned Si wafers. Prior to SWNT thin film transfer, thermal oxide (500 nm) grown Si wafers were patterned with Cr/Au by photolithography (top contact and etch mask). Top Si windows were exposed by the wet-etch of the oxide, and back contacts were fabricated using Al. The SWNT thin films floating on the water were picked up by the top/back-patterned Si wafers. The fabricated SWNT/Si windows were treated with hydrofluoric acid (HF), then nitric acid to optimize the photovoltaic properties. Subsequently, they were treated with gold salt (gold(III) chloride hydrate in nitromethane) which further p-dopes the SWNTs. Both steps are critical to achieve high efficiencies (Supporting Information, S1). The completed SWNT/Si solar cell has the architecture of a typical single junction single crystalline p−n Si solar cell except that the emitter layer is replaced by a thin SWNT film.

Figure 1a illustrates the schematic of a SWNT/Si solar cell. Figure 1b is a photograph to show a SWNT thin film on a slide glass prior to transfer to a Si wafer, prepared by the superacid sliding coating method. Figure 1c top shows the plane-view scanning electron microscopy (SEM) image of a representative SWNT thin film revealing highly aligned SWNTs. The bottom SEM image of a cross-sectioned SWNT/Si interface (60° tilted) shows a conformal coating of SWNTs on the Si surface. Figure 1d shows the current density (J)−voltage (V) characteristics of a representative SWNT/Si solar cell under 1 sun (P_{input} = 100 mW/cm^2, AM 1.5 illumination). The extracted device parameters are as follows; the short circuit current density (J_{sc}) is 28.6 mA/cm^2, open circuit voltage (V_{oc}) is 530.1 mV, and the fill factor (FF) is.74.1%, which results in the PCE of 11.2%. This high FF of 74.1% is comparable to the highest reported FF of >75% observed in a "wet-state" CNT/Si solar cell.[5] Our optimized solar cells exhibit PCE in a typical range of 11−11.5%.[11] To the best of our knowledge, these values are greater than the PCEs of any organic/Si hybrid solar cells reported so far, exceeding the high PCE (11.1%) of the poly(3,4-ethylene dioxythiophene):poly-(styrenesulfonate) (PEDOT:PSS)/Si nanocone hybrid solar cells recently developed with conventional microelectronic processes.[12]

To understand the observed high efficiency, we investigate the carrier transport mechanism by employing temperature-dependent electrical characterization (Janis Instruments cryostat). Figure 2a shows the dark forward J−V characteristics of a SWNT/Si solar cell with varying temperature T, revealing the increase of J with increasing T. The device ideality factor, n, is determined under forward bias, and the linear fit to the plot of ln(J)−V at its linear regime (Figure 2a, inset) yields the ideality factor of 1.09 at 310 K. The room-temperature ideality factor of our solar cells with >11% efficiency is typically in a range of ~1.05−1.15 (n = 1.1 for the device in Figure 2a), significantly smaller than those previously reported ($1.4 < n < 3.8$) for any CNT/Si solar cells.[2] These values close to unity are a feature of transport characteristics with minimum interface recombination, as further discussed later. With high revere biases applied, the devices typically undergo nondestructive reverse breakdown, as demonstrated with another device (Figure 2b). The reverse breakdown voltage also increases with increasing temperature, which indicates an avalanche breakdown mechanism owing to the ionization impact of charge carriers, generally observed in lightly doped p−n junction devices;[13] as the temperature increases, the mean free path of carriers

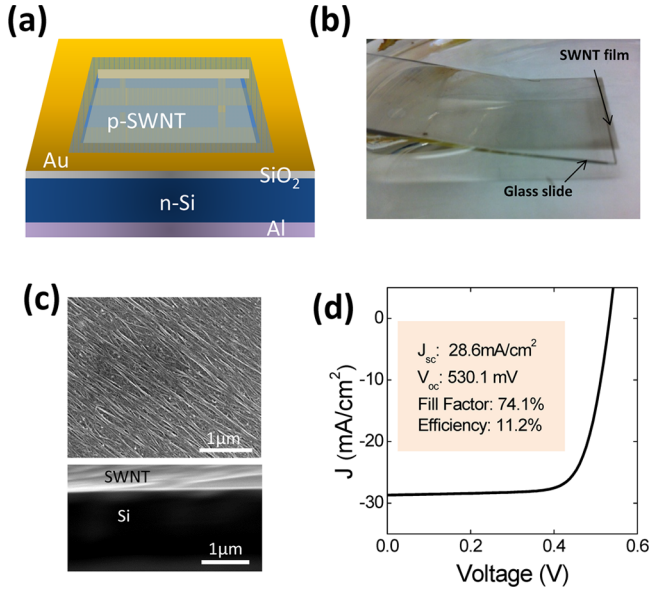

Figure 1. (a) Schematic of a SWNT/Si hybrid solar cell. (b) Photograph to show a SWNT thin film prepared on a slide glass for transfer to a Si wafer. (c) Plane-view of a representative SWNT film (top) and cross-sectioned view of SWNT/Si interface (bottom). (d) J−V characteristics of a SWNT/Si solar cell under 1 sun illumination, exhibiting a PCE of 11.2%.

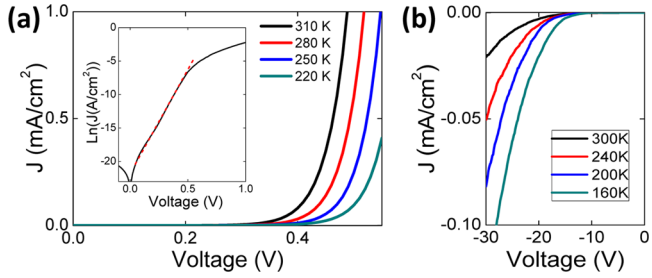

Figure 2. (a) Temperature-dependent forward J−V characteristics of a SWNT/Si solar cell. Inset shows the semilogarithmic plot of J−V at 310 K and its linear fit. (b) Temperature-dependent reverse breakdown characteristics.

dx.doi.org/10.1021/nl3035652 | Nano Lett. 2013, 13, 95−99

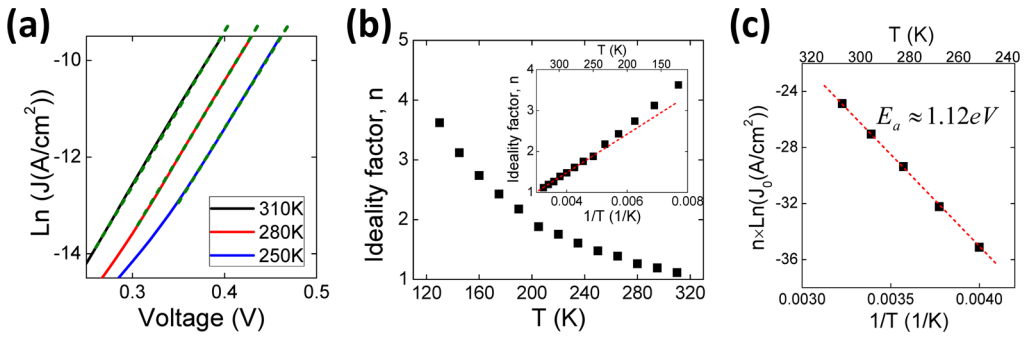

Figure 3. (a) Determination of ideality factor from the semilogarithmic plots of $J-V$ at varying temperatures. (b) Variation of ideality factor, n, with varying temperature, T. Inset shows the plot of n vs $1/T$. (c) Plot of $n \times \ln(J_0)$ vs $1/T$ to extract the activation energy of ∼1.12 eV.

decreases, thereby requiring a higher electric field for acquiring sufficeint energy for ionization. In p−n junction devices with avalanche reverse breakdown, the reverse breakdown voltage V_{br} at a certain temperature T is known to be $V_{br}(T) = V_{br}(T_0)[1 + \beta(T - T_0)]$, where T_0 is room temperature and β is the temperature coefficient.[14] We calculate β as $\sim 1.1 \times 10^{-3}$ (K^{-1}), which is in good agreement with the values for p−n junction Si solar cells (a typical range of -10^{-4} (K^{-1}) to 10^{-3} (K^{-1})).[15]

The device ideality factor, n, is determined at various temperatures from the linear regime of each $\ln(J)-V$ plot yielding the largest slope (where $V > qkT$),[13] shown in Figure 3a. It is observed to increase with decreasing temperature, as shown in Figure 3b. The increase of the ideality factor with decreasing temperature, T, has been observed in a variety of p−n hetero (or homo) junction solar cells such as organic/organic,[16] organic/inorganic,[17] and inorganic/inorganic heterojunction solar cells[18] as well as Si-based homo[19] or heterojunction[20] solar cells. Such temperature dependency is generally explained by tunneling-enhanced recombination models[21,22] which take into account the tunneling-enhanced recombination rates of charge carriers via bulk recombination centers having an exponential distribution in energy. These models predict a linear relationship in $1/n$ vs T at moderately high temperature where the contribution of the tunneling is less dominant, which is in an agreement with our observation (Figure 3b, inset). Some deviation from linearity at low temperature (<∼190 K) is attributed to enhanced tunneling.

The dark forward $J-V$ characteristics are empirically expressed as $J = J_0 \exp(qV/nkT)$ where J_0, n, k, T, and q represent the saturation current density, device ideality factor, Boltzmann constant, temperature, and unit charge, respectively.[13] The saturation current density J_0 is expressed as $J_0 = J_{00} \exp(-E_a/nkT)$ for p−n junctions, where J_{00} is the temperature-independent prefactor and E_a is the thermal activation energy barrier responsible for current rectification.[13] This equation predicts a linear relationship in the plot of $n \times \ln(J_0)$ vs $1/T$, where its linear slope yields the activation energy E_a.[16−18,20−22] In organic/Si heterojunction solar cells, it is known that E_a is related to the band gap energy (E_g) of light absorbing materials (diffusion transport) or interfacial barrier height at which charge carriers recombine (interface recombination transport).[23] The saturation current density J_0 is determined by the intercept of the linear fit in the plot of $\ln(J)$ vs V extrapolated to zero-bias.[16,17] Figure 3c shows the plot of $n \times \ln(J_0)$ vs $1/T$ in the temperature range of 310−250 K where E_a is determined to be ∼1.12 eV. This value matches well with the band gap of Si in this temperature range,[13] suggesting that the temperature-dependent rectifying characteristics originate from the thermally generated/activated intrinsic carriers in Si, and that Si is the light-absorbing/photocarrier generating active site in the SWNT/Si solar cells. This large activation energy rules out the possibility of the MS Schottky junction model for our devices, as further discussed later. The role of the SWNT thin film is to establish a built-in potential for carrier separation/transport and its contribution to photocarrier generation is insignificant, as implied by its very high transmittance (which should be >90% at 550 nm wavelength).[24] Recent optical characterization of incident photon-to-charge carrier efficiency with similarly structured-SWNT/Si solar cells also revealed dominant absorption peaks near the band gap of Si.[9,25] In addition, by extracting E_a and J_{00}, we predict V_{oc} to be ∼0.52 eV using $V_{oc} = E_a/q - nkT/q \times L_n(J_{00}/J_{sc})$[16,26] which is close to the experimentally measured value. We note that the above methodology to extract the band gap of light absorbing materials using the activation energy plot have extensively been employed in investigating the carrier transport mechanisms of a variety of heterojunction solar cells.[18,21,22,27,28] In fact, the dominant photocarrier generation in Si has been identified in various organic/Si hybrid solar cells by correlating E_a with the band gap of Si, while these solar cells exhibit recombination-dominated carrier transports with large ideality factors.[29,30]

In the general p−n junction model, the total dark-current density J_t constitutes the diffusion current density J_d (diffusion of carriers in neutral regions, i.e., bulk recombination) and the generation−recombination current density J_r (thermal generation−recombination of carriers inside space-charge regions, i.e., interface recombination).[13] When J_r is insignificant, J_t becomes dominated by J_d, and the device ideality factor becomes close to unity. In this case, the temperature dependence of J_t is primarily determined by the intrinsic carrier concentration n_i of the light absorbing material; thus its band gap energy, since $J_t \approx J_d \propto n_i^2 \propto \exp(-E_g/k_T)$. The ratio of the recombination current vs the diffusion current is known to be $J_r/J_d \approx (n-1)/(1-0.5n)$,[31] which yields ∼81% of J_d with n = 1.1, further confirming that the transport is dominated by diffusion. This diffusion-dominated transport with suppressed generation−recombination current are responsible for the enhanced efficiency of the devices, similarly observed in high-efficiency heterojunction intrinsic thin layer (HIT) p−n Si solar cells, as revealed by the plot of $n \times \ln(J_0)$ vs $1/T$.[27,28]

We note that our solar cells exhibit the enhanced contribution of interface carrier recombination at low forward bias, which becomes more pronounced with decreasing temperature. The close-up view of the forward $\ln(J)-V$ plots (310 and 220 K) at <0.5 V reveals two distinct linear regimes

dx.doi.org/10.1021/nl3035652 | Nano Lett. 2013, 13, 95−99

separated at high/low bias in each plot (Supporting Information, S2a). The low bias-linear regimes yields smaller slopes than those from the high bias-linear regimes (diffusion-dominated), which represents the increase of interface recombination.[32] Moreover, the value of the V which separates the two linear regimes also increases with decreasing temperature, similar to the transport characteristics of various p−n Si solar cells.[27,28,32,33] The activation energy plot (Supporting Information, S2b) obtained from the low bias regime yields $E_a \sim 0.91$ eV, smaller than that from the diffusion regime, indicating an increase of interface recombination (E_a should be $E_g/2-0.56$ if the transport is dominated by interface recombination only[13]). Thus, at low temperature and low bias, interface carrier recombination can occur, but under the normal operating condition of our solar cells (i.e., at/near room temperature and forward bias with $V > qkT$), diffusion transport dominates.

To further support the diffusion-dominated carrier transport, we characterized the minority carrier recombination lifetime of these cells by using the reverse recovery transient method.[34,35] The p−n junction diode is operated by abruptly switching forward-to-reverse bias, and the resultant transient response directly corresponds to the lifetime of minority carriers (Figure 4 inset). Figure 4 shows the room-temperature recovery

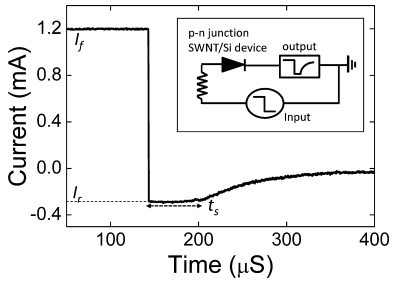

Figure 4. Reverse recovery transient characteristic of a SWNT/Si solar cell. The inset illustrates the schematic of the measurement setup.

transient characteristic from the same device in Figure 2a. The current response shows three distinct phases of constant forward current (I_f), constant reverse current (I_r) for a short period of time (t_s), and slow decay/saturation of the reverse current, yielding the minority carrier lifetime, τ, to be $\tau = t_s/[\ln(1 + I_f/I_r)]$.[34] From this equation and Figure 4, the minority carrier lifetime is determined to be ∼34 μs. We can compare this to the carrier lifetime theoretically estimated from the forward-bias device characteristics for diffusion-dominated carrier transport.[31] By differentiating J_t with respect to V, one can obtain $(\partial J_t/\partial V)|_{V=0} \approx (q/k_T)(qn_{iSi}^2/N_D)[(D_p/\tau)^{1/2}]$ where N_D is the doping concentration of Si, D_p is the diffusion coefficient of holes, and τ is the lifetime. Using $n_i = 1.1 \times 10^{10}$ cm^{-3}, $N_D = 1.5 \times 10^{15}$ cm^{-3}, and $D_p = 12$ cm^{-2} s^{-1}, we estimate the lifetime to be ∼18 μs, in reasonable agreement with the measured value. All of these observed device characteristics, that is, the small ideality factor, long carrier lifetime, and diffusion-dominated transport, strongly indicate the suppression of interface recombination. It is encouraging that our low-cost/hybrid approach is capable of forming high-quality p−n junction, which has conventionally relied on conventional Si microfabrication, such as ion implantation and high-temperature/vapor-phase processes.

Of the three potential device models (p−n heterojunction, MS Schottky junction, or MIS Schottky junction), the easiest to rule out is MS Schottky junction model which is expressed by $J \propto A^*T^2 \exp(-\phi/nKT)$, where A^* is the Richardson constant and Φ is Schottky barrier height.[13] The Schottky barrier height can be determined from the Richardson plot of $n \times \ln(J/T^2)$ vs $1/T$ under varying temperature. The Richardson plot with our data yields an activation energy value of ∼1.56 eV, significantly greater than the theoretically predicted (or experimentally measured) SWNT/Si Schottky barrier height[2,36] (Supporting Information, S4). A second piece of evidence is the small value of the dark saturation current density J_0 (∼7×10^{-11} A cm^{-2} at room temperature) observed in our solar cells. It is well-known that the J_0 of MS Schottky solar cells are much larger than those of p−n junction solar cells, due to the lower Schottky barrier height.[12,37] We note that J_0 of various carbon-based thin film/Si hybrid Schottky devices at room temperature are much larger than that of our SWNT/Si solar cell, such as graphene/Si Schottky junction solar cells ($J_0 \sim 1 \times 10^{-8}$ A cm^{-2}) irrespective of the chemical doping of the graphene,[38,39] or conjugated polymer/Si Schottky junction solar cells ($J_0 \sim 1 \times 10^{-7}$ A cm^{-2}).[12] Even with the much smaller J_0 of our solar cells, we still have V_{oc} values comparable to those of CNT/Si (or carbon/Si) MS Schottky junction solar cells, mainly due to the much smaller ideality factor of our devices. For example, using $V_{oc} = nkT/q \times L_n(J_{sc}/J_s)$, we calculate V_{oc} to be ∼0.56 V for our devices, which compares well to the graphene/Si Shocttky junction solar cells which have V_{oc} (calculation) ∼0.50−0.57 V (the range due to uncertainty in ideality factor) and V_{oc} (experiment) = 0.54 V.[38] Finally, a measurement of the capacitance (C)−voltage (V) characteristics yields a linearity in the $1/C^2-V$ plot (Supporting Information, S3), which is consistent with the characteristic of a highly asymmetric p−n junction.

The characteristics of MIS Schottky junction devices are similar to those of p−n junction devices, since both are based on minority carrier transport and similar activation energies are possible.[40,41] In Si-based MIS solar cells, the insertion of a thin SiO_x in between Si and metal is essential for efficient charge carrier separation, and minority carrier transport through this insulating layer is based on tunneling. Such a transport mechanism has been claimed with CNT/Si solar cells where improved device characteristics were observed with SiO_x on the Si surface.[42] However, our SWNT/Si solar cells show opposite characteristics—namely, the closer-to-unity ideality factor and enhanced PCE by removal of SiO_x with HF. Without the removal of the SiO_x (after SWNT deposition), device parameters (n, J_{sc}, and FF) significantly degraded, inconsistent with a MIS Schottky junction model. Also, it is important to note that our nitric acid treatments are not likely to introduce a SiO_x layer thick enough (>1 nm) for the formation of the MIS structure[41] owing to their mild process conditions (∼3 wt %, room temperature, 20 s duration).[43]

In summary, we have fabricated SWNT/Si solar cells with a record high PCE of >11% for CNT/Si solar cells. By employing temperature-dependent electrical characterizations, we have revealed diffusion-dominated p−n junction transport and dominant photocarrier generation in Si. This study suggests that the superior photovoltaic properties of single-crystalline Si can be realized by a simple, low-temperature process, thus implying a great potential for low-cost, high-efficiency solar cells. The fact that high PCE can be achieved without a need for complicated processing of CNTs (such as sorting-out of nanotube type) is very encouraging for further utilization of CNTs for various photovoltaic applications.

dx.doi.org/10.1021/nl3035652 | Nano Lett. 2013, 13, 95−99

■ ASSOCIATED CONTENT

Supporting Information

Post-treatment of SWNT/SI windows, J−V characteristics at low voltage, capacitance−voltage measurement, and Richardson plot. This material is available free of charge via the Internet at http://pubs.acs.org.

■ AUTHOR INFORMATION

Corresponding Author

*E-mail: yeonwoong.jung@yale.edu, andre.taylor@yale.edu. Telephone number: +1 (203) 432-2217. Fax number: (203) 432-4387.

Author Contributions

§These authors equally contributed to the work.

Notes

The authors declare no competing financial interest.

■ ACKNOWLEDGMENTS

This work was supported by the SOLAR program of the National Science Foundation under DMR-0934520. Support is also acknowledged from the NSF-CAREER award CBET-0954985 and NASA (CT Space Grant Consortium). This research was supported as part of the Nanostructures for Electrical Energy Storage, an Energy Frontier Research Center funded by the U.S. Department of Energy, Office of Science, Office of Basic Energy Sciences under Award Number DESC0001160 (Y.J.). Facilities used were supported by Yale Institute for Nanoscience and Quantum Engineering and NSF MRSEC DMR 1119826. The authors acknowledge Dr. Nilay Hazari for helpful discussions and use of facilities for superacid preparation and processing. Southwest Nanotechnologies is acknowledged for their kind supply of single walled carbon nanotubes. We also thank Xiao Sun and the T. P. Ma group for assistance with $C-V$ measurements.

■ REFERENCES

(1) Léonard, F. *The physics of carbon nanotube devices*; William Andrew: New York, 2009.

(2) Tune, D. D.; Flavel, B. S.; Krupke, R.; Shapter, J. G. *Adv. Energy Mater.* **2012**, DOI: 10.1002/aenm.201200249.

(3) Jia, Y.; Cao, A.; Bai, X.; Li, Z.; Zhang, L.; Guo, N.; Wei, J.; Wang, K.; Zhu, H.; Wu, D.; Ajayan, P. M. *Nano Lett.* **2011**, *11*, 1901.

(4) Jia, Y.; Li, P.; Gui, X.; Wei, J.; Wang, K.; Zhu, H.; Wu, D.; Zhang, L.; Cao, A.; Xu, Y. *Appl. Phys. Lett.* **2011**, *98*, 133115.

(5) Wadhwa, P.; Liu, B.; McCarthy, M. A.; Wu, Z.; Rinzler, A. G. *Nano Lett.* **2010**, *10*, 5001.

(6) Wadhwa, P.; Seol, G.; Petterson, M. K.; Guo, J.; Rinzler, A. G. *Nano Lett.* **2011**, *11*, 2419.

(7) Li, Z.; Kunets, V. P.; Saini, V.; Xu, Y.; Dervishi, E.; Salamo, G. J.; Biris, A. R.; Biris, A. S. *ACS Nano* **2009**, *3*, 1407.

(8) Ong, P.-L.; Euler, W. B.; Levitsky, I. A. *Nanotechnology* **2010**, *21*, 105203.

(9) Li, Y.; Kodama, S.; Kaneko, T.; Hatakeyama, R. *Appl. Phys. Expr.* **2011**, *4*, 065101.

(10) In this work, we report dry-state measurements only to emphasize intrinsic device characteristics. Wet-state characteristics of our solar cells have shown efficiencies as large as >18% at 1 sun (ref 11).

(11) Li, X., et al., submitted.

(12) Jeong, S.; Garnett, E. C.; Wang, S.; Yu, Z.; Fan, S.; Brongersma, M. L.; McGehee, M. D.; Cui, Y. *Nano Lett.* **2012**, *12*, 2971.

(13) Sze, S. M.; Ng, K. K. *Physics of Semiconductor Devices*, 3rd ed.; Wiley: New York, 2007.

(14) McKay, K. G. *Phys. Rev.* **1954**, *94*, 877.

(15) Mahadevan, S.; Hardas, S. M.; Suryan, G. *Phys. Status Solidi A* **1971**, *8*, 335.

(16) Stevens, D. M.; Speros, J. C.; Hillmyer, M. A.; Frisbie, C. D. *J. Phys. Chem. C* **2011**, *115*, 20806.

(17) Koster, L. J. A.; Mihailetchi, V. D.; Ramaker, R.; Blom, P. W. M *Appl. Phys. Lett.* **2005**, *86*, 123509.

(18) Rau, U.; Jasenek, A.; Schock, H. W.; Engelhardt, F.; Meyer, T. *Thin Solid Films* **2000**, *298*, 361.

(19) Rahmouni, M.; Datta, A.; Chatterjee, P.; Damon-Lacoste, J.; Ballif, C.; Cabarrocas, P. R. I. *J. Appl. Phys.* **2010**, *107*, 054521.

(20) Nolasco, J. C.; Cabré, R.; Ferré-Borrull, J.; Marsal, L. F.; Estrada, M.; Pallarès, J. *J. Appl. Phys.* **2010**, *107*, 044505.

(21) Rau, U. *Appl. Phys. Lett.* **1999**, *74*, 111.

(22) Nadenau, V.; Rau, U.; Jasenek, A.; Schock, H. W. *J. Appl. Phys.* **2000**, *87*, 584.

(23) Nolasco, J. C.; Cabré, R.; Ferré-Borrull, J.; Marsal, L. F.; Estrada, M.; Pallarès, J. *J. Appl. Phys.* **2010**, *107*, 044505.

(24) Li, X.; Gittleson, F.; Carmo, M.; Sekol, R. C.; Taylor, A. D. *ACS Nano* **2012**, *6*, 1347.

(25) Bai, X.; Wang, H.; Wei, J.; Jia, Y.; Zhu, H.; Wang, K.; Wu, D. *Chem. Phys. Lett.* **2012**, *70*, 533.

(26) Gunawan, O.; Todorov, T. K.; Mitzi, D. B. *Appl. Phys. Lett.* **2010**, *97*, 233506.

(27) Jensen, N.; Rau, U.; Hausner, R. M.; Uppal, S.; Oberbeck, L.; Bergmann, R. B.; Werner, J. H. *J. Appl. Phys.* **2000**, *87*, 2639.

(28) Taguchi, M.; Maruyama, E.; Tanaka, M. *Jpn. J. Appl. Phys.* **2008**, *47*, 814.

(29) El-Nahass, M. M.; Metwally, H. S.; El-Sayed, H. E. A.; Hassanien, A. M. *Synth. Met.* **2011**, *161*, 2253.

(30) El-Nahass, M. M.; Abd-El-Rahman, K. F.; Farag, A. A. M.; Darwish, A. A. A. *Org. Electron.* **2005**, *6*, 129.

(31) Vanhellemont, J.; Simoen, E.; Claeys, C. *Appl. Phys. Lett.* **1995**, *66*, 2894.

(32) Michaelis, W.; Pilkuhn, M. H. *Phys. Status Solidi* **1969**, *36*, 311.

(33) Garlick, G. F. J.; Kachare, A. H. *Appl. Phys. Lett.* **1980**, *36*, 911.

(34) Kuno, H. J. *IEEE Trans. Electron Devices* **1964**, *11*, 8.

(35) Jung, Y.; Vacic, A.; Perea, D. E.; Picraux, S. T.; Reed, M. A. *Adv. Mater.* **2011**, *23*, 4306.

(36) Behnam, A.; Radhakrishna, N. A.; Wu, Z.; Ural, A. *Appl. Phys. Lett.* **2010**, *97*, 233105.

(37) Avasthi, S.; Lee, S.; Loo, Y.-L.; Sturm, J. C. *Adv. Mater.* **2011**, *23*, 5762.

(38) Miao, X.; Tongay, S.; Petterson, M. K.; Berke, K.; Rinzler, A. G.; Appleton, B. R.; Hebard, A. F. *Nano Lett.* **2012**, *12*, 2745.

(39) Li, X.; Zhu, H.; Wang, K.; Cao, A.; Wei, J.; Li, C.; Jia, Y.; Li, Z.; Li, X.; Wu, D. *Adv. Mater.* **2010**, *22*, 2743.

(40) Tarr, N. G.; Pulfrey, D. L. *Appl. Phys. Lett.* **1979**, *34*, 295.

(41) Shewchun, J.; Singh, R.; Green, M. A. *J. Appl. Phys.* **1977**, *48*, 765.

(42) Jia, Y.; Cao, A.; Kang, F.; Li, P.; Gui, X.; Zhang, L.; Shi, E.; Wei, J.; Wang, K.; Zhu, H.; Wu, D. *Phys. Chem. Chem. Phys.* **2012**, *14*, 8391.

(43) Asuha, H. K.; Maida, O.; Takahashi, M.; Iwasa, H. *J. Appl. Phys.* **2003**, *94*, 7328.